Archaeological and Anthropological Sciences
https://doi.org/10.1007/s12520-018-0710-y

ORIGINAL PAPER

The mechanical properties of heat-treated rocks: a comparison between chert and silcrete

Patrick Schmidt[1,2] · Gerald Buck[2] · Christoph Berthold[2,3] · Christoph Lauer[2] · Klaus G. Nickel[2,3]

Received: 27 June 2018 / Accepted: 12 September 2018
© Springer-Verlag GmbH Germany, part of Springer Nature 2018

Abstract

In archaeology, heat treatment of stone is the process of "making" a new material for tool production. Its invention in the African Middle Stone Age was an important step in the evolution of transformative technologies and the cultural evolution of early humans in general. Although the chemical and crystallographic transformations in silica rocks, the only material class heat-treated in the Stone Age, begin to be well known, many of the mechanical transformations and their chemical origins remain a subject of controversy. The difference between different silica rock categories is also only poorly understood. In this paper, we investigate the thermally induced changes of three mechanical properties in the two silica rock types chert and silcrete: fracture strength, indentation fracture resistance (approximating fracture toughness) and elastic modulus. These tests are complemented by statistical analyses (Weibull modulus) and a quantitative fracture surface analysis. The results show that heat treatment transforms these silica rocks in terms of their fracture toughness and the uniformity of fracture. A comparison with published data on the structural transformations in the same samples identified the loss of chemically bound water and subsequent defect healing to be the chemical mechanism behind these mechanical transformations. These findings have important implications for the study of the interactions between chemical and structural processes and the mechanics of natural rocks or ceramics.

Keywords Bending tests · Indentation fracture resistance (IFR) · Crystallography of tool stones · Knapping quality · Archaeology

Introduction

In prehistoric archaeology, heat treatment of stone to produce tools by controlled fracturing (stone knapping) is commonly understood as one of the earliest efforts of humankind to deliberately alter the properties of naturally available materials. The earliest examples date back to the African Middle Stone Age (Brown et al. 2009; Porraz et al. 2013; Mourre et al. 2010; Schmidt and Mackay 2016; Delagnes et al. 2016; Schmidt et al. 2015) and were interpreted to be a proxy for "modern behaviour" (McBrearty and Brooks 2000; Sealy 2009) or "complex cognition" (Wadley 2013). In later periods, heat treatment is often interpreted as marker of high technical skill (Tiffagom 1998; Inizan and Tixier 2001) or specialised craftsmanship (Léa et al. 2012). Although the first recognition of stone heat treatment in archaeological contexts dates back to the 1960s (Crabtree and Butler 1964; Shippee 1963; Bordes 1969), a critical review of the available literature reveals that the processes taking place in stone are not completely understood yet: most of the available studies concern the mineralogical, chemical or crystallographic transformations (Purdy 1974; Purdy and Brooks 1971; Flenniken and Garrison 1975; Mandeville 1973; Domanski et al. 2009; Domanski and Webb 1992; Griffiths et al. 1987; Schmidt et al. 2012b, 2013b), but only few detailed data on the thermal evolution of fracture mechanics have been published to date (see for example Domanski et al. 1994; Schindler et al. 1982; Kerkhof and Müller-Beck 1996). It thus appears necessary to investigate in more detail the influence of heat treatment on the mechanical properties of the rocks used for heat treatment in prehistory.

A variety of heated rocks, like sandstone (Hurst et al. 2015), shale (Yonekura 2010), quartzite (Ebright 1987) or

✉ Patrick Schmidt
patrick.schmidt@uni-tuebingen.de

[1] Department of Prehistory and Quaternary Ecology, Eberhard Karls University of Tübingen, Schloss Hohentübingen, 72070 Tübingen, Germany

[2] Department of Geosciences, Applied Mineralogy, Eberhard Karls University of Tübingen, Wilhelmstraße 56, 72074 Tübingen, Germany

[3] Competence Center Archaeometry–Baden Wuerttemberg, Eberhard Karls University of Tübingen, Wilhelmstraße 56, 72074 Tübingen, Germany

Published online: 20 September 2018

silicified tuff (Kononenko et al. 1998), have been mentioned, but the vast majority of all heat-treated archaeological assemblages are made of only two categories of silica rocks: chert and silcrete. The former is a fine-grained marine rock made of chalcedony, a nano-crystalline quartz texture with fibre-like structure (Cady et al. 1998; Rios et al. 2001; Flörke et al. 1991). Several nomenclatures describing such rocks are available (Füchtbauer 1988; Cayeux 1929; Tucker 1991) and the terms flint (for cretaceous rocks formed in chalk) and more generally chert appear regularly throughout the literature. We use 'chert' here to address chalcedony-rich rocks in general, while stressing that no particular geological background can be inferred from this term. The other category, silcrete, is a continental sub-surface rock formed by the concretion of pre-existing sediments by secondary quartz cement (Summerfield 1981, 1983) (the minerals from the original sediments, mainly quartz, are preserved as clasts in the rocks). The cement may be chalcedony in groundwater silcrete (Nash and Ullyott 2007; Thiry 1991), but in (archaeologically more common) pedogenic silcrete (Summerfield 1981; Roberts 2003), it normally is micro-quartz. Thus, chert and silcrete are both formed by quartz and the main difference is grain size and therefore the micro-structure. These differences have important implications for the density of defects like pores in both rocks. For example, silcrete was reported to contain up to five times more pore-space than chert (compare Schmidt et al. 2011, 2013b, 2017a, b). This pore-space is mostly intergranular in chalcedony (Fukuda et al. 2009; for a counterexample, see Milot et al. 2017), while in silcrete, both intergranular pores and supplementary macro-pores (Summerfield 1983) may be present. Chert was also shown to contain more chemically bound water (silanol, SiOH) than most silcrete (again compare Schmidt et al. 2011, 2013b, 2017a, b). In both rocks, SiOH can be expected to occur at crystal defects, low angle grain boundaries and on pore walls (Graetsch et al. 1985; Flörke et al. 1982; Schmidt et al. 2017a, b; Miehe et al. 1984), effectively lowering the coherence between grains. Upon heat treatment, the transformations of these 'water'-related defects were shown to be similar in chalcedony and micro-quartz (compare Schmidt et al. 2011, 2017a, b): when a minimal activation temperature is reached (normally ≥ 200 °C, Schmidt et al. 2013c), water is progressively expelled from the structure, allowing for the formation of new Si-O–Si bonds. In chalcedony, these new bonds were shown to increase nano-hardness (Schmidt et al. 2012b), and in both rocks, they are strongly suspected to cause the observed improvement of knapping quality after heat treatment (Schmidt et al. 2012b, 2013b).

Whether this is really the case, or whether it is other factors that influence the heat-induced mechanical transformations, may be understood if some of the fundamental mechanical properties involved in stone knapping are investigated in samples for which these 'water'-related transformations are already known. In this paper, we therefore analyse a set of chert and silcrete samples for which the chemical and crystallographic transformations have already been published (Schmidt et al. 2013a, 2017a, b). We use bending tests to investigate fracture strength, indentation testing to investigate fracture resistance and resonant damping analysis to investigate the evolution of Young's modulus. These tests are complemented by a quantitative analysis of fracture surfaces from unheated and heated samples. Correlating both datasets, our mechanical data and the published chemical data, we attempt to answer three specific questions:

- Which mechanical properties are transformed upon heat treatment and at what temperatures?
- Are the heat-induced mechanical transformations similar in chert and silcrete? If so, how do both materials compare quantitatively in terms of these transformations?
- What are the chemical or crystallographic mechanisms that trigger these transformations?

Materials and methods

Samples and sample preparation

One sample of chert from the Vaucluse region of France and three samples of silcrete from the West Coast region of South Africa were analysed. We chose these samples because rocks coming from these locations were used as raw materials and heat-treated to produce stone tools in different archaeological chrono-cultural periods: chert from the Vaucluse (locally called silex barremo-bédoulien) was systematically heat-treated and pressure-knapped in the Neolithic Chassey culture (Léa 2005); silcrete from the three sampled outcrops was heat-treated and subsequently knapped to produce tools in the nearby Middle Stone Age site of Diepkloof Rock Shelter (Porraz et al. 2013; Schmidt et al. 2015) and the Late Stone Age site of Elands Bay Cave (Porraz et al. 2016). There is detailed published data on the 'water'-related thermal transformations of the three silcrete samples (Schmidt et al. 2017a) and some aspects of these transformations, recorded in two samples coming from the same outcrop as our chert sample, are available (Schmidt et al. 2013a, 2016). Chert is a rather homogenous rock and we expect that the dehydration data obtained on identically looking samples, coming from a few metres away in the same outcrop, can be transferred to our chert sample. In this way, the mechanical properties measured in this study can be compared with the 'water'-related thermal transformations of the samples. Sample numbers and descriptions, as extracted from Schmidt et al. (2016, 2017a), are summarised in Table 1.

To measure the elastic modulus and fracture strength of these samples, a varying number of bending bars were

Table 1 Sample origins, descriptions, 'water' content and pore space as extracted from Schmidt et al. (2016, 2017a) (*m* = mass; LF = length-fast; LS = length-slow)

Sample number	Location and age	Description and origin	*m* SiOH (wt%)	*m* H_2O (wt%)	Pores (vol%)
VC-12-05 (chert)	France, near the town of Malaucène. Barremian to lower Abtian.	Light-brown to yellowish chert from solid limestone, ~ 85% LF-chalcedony, ~ 15% LS-chalcedony, minor detrital quartz grains and dispersed opal-CT lepidospheres.	0.56 ± 0.01	0.33 ± 0.01	0.65 ± 0.1
WK-13-08 (silcrete)	South Africa, West Coast, near the town of Hopefield. Undated.	Silcrete with a floating texture. Clasts: 32 vol% with average size 0.2 mm. Crystal size cement > 5 μm.	0.43 ± 0.01	0.36 ± 0.01	3.39 ± 0.1
WK-13-11 (silcrete)	South Africa, West Coast, near the town of Velddrif. Undated.	Silcrete with a floating to grain supported structure. Clasts: 58 vol% with average size 0.19 mm. Crystal size cement ≈ 7 μm.	0.1 ± 0.01	0.13 ± 0.01	0.69 ± 0.1
WK-13-13 (silcrete)	South Africa, West Coast, near the town of Redelinghuys. Undated.	Silcrete with grain supported structure. Clasts: 66 vol% with average size 0.92 mm. Crystal size cement ≈ 12 μm.	0.05 ± 0.01	0.09 ± 0.01	0.26 ± 0.1

prepared from each sample (Silcretes WK-13-08: 50; -11: 49; -13: 54 and Chert VC-12-05: 35). Bending bars were prepared by water jet cutting to avoid mechanical stresses in the samples that might influence their fracture behaviour. Bending bar dimensions were chosen to account for different grain- and clast-sizes in chert and silcrete: 42 × 4.5 × 4.3 mm for chert VC-12-05 and the relatively fine-grained silcrete WK-13-08; 42 × 8.0 × 7.8 mm for both coarser-grained silcrete samples WK-13-11 and -13. All faces on these bending bars were ground and lapped with the aid of 46 μm diamonds as abrasives to be plane-parallel and two edges were chamfered on the bars' tension side to remove chips on the edges that may influence the fracture behaviour. For the chert sample, indentation fracture resistance (IFR) was measured my means of indentation on the surface of these bending bars. To measure IFR in silcrete, two separate ~ 20 × ~ 30 × ~ 5 mm measuring plane-parallel plates were cut, and diamond polished on one side, from samples WK-13-08 and -13.

Experimental protocol

During all experiments, the lowest heating increment was 110 °C; no "unheated" measurements were made. The reason for this is that we expected that, despite of systematically applied water cooling during manufacturing, cutting of the bending bars and polishing of the plates for indentation may have slightly heated the samples. To homogenise initial temperatures before the heating sequences, all samples were stored in a drying oven at 110 °C for 2 days before the experiments began. All further heating steps were conducted in oxidising atmosphere using an electrical furnace. The heating rate used for all temperature steps was ≤ 1.5 °C/min to avoid unwanted fracturing (Schmidt 2014); samples were held at maximum temperature for 4 h (based on the results in Schmidt et al. 2012a, 2016); cooling rate was ≤ 0,68 °C/min to avoid fracturing caused by too rapid cooling.

Elastic modulus

Elastic modulus, or Young's modulus (*E*), was measured on bending bars by means of non-destructive resonant frequency damping analysis (RFDA) at room temperature following DIN EN 843 2 (2006). During these tests, bending bars are excited by a mechanical impulse, upon which they oscillate with one or several resonant frequencies. The resulting signal is recorded with a microphone to calculate *E* from the sample's damping behaviour. The protocol began by measuring *E* for all bending bars. One bending bar of each sample was then heat-treated with the first temperature step, reanalysed after cooling to room temperature and then heated to the next step (temperature steps for this sequence were 150 to 600 °C with 50 °C increments). All measurements were made before atmospheric water could re-adsorb in the pore-space (transport in a silica gel dried atmosphere prevented the samples from hydrating before the measurements); hence, they reflect the samples' elastic properties in a dehydrated state. To investigate whether this sequential heating to successive temperatures is comparable to single heating events, 3 sets of 7 bending bars of the chert sample VC-12-05 and 4 sets of 10 bending bars cut from each of the three WK-silcrete samples were heated to different temperatures (VC-sample: 250 °C, 300 °C, 350 °C; WK-samples: 250 °C, 350 °C, 450 °C, 600 °C) and analysed in the RFDA unit (one bar of WK-13-08 and one of − 11 heated to 600 °C broke so that *E* could only be measured on 9 bars heated to this temperature step). This second set of measurements was then compared with the results obtained from the continuous stepwise heating sequences to evaluate whether multiple heating cycles and increasing temperature steps have an influence on the evolution of Young's modulus.

It should be noted that measurements of *E* in the chert sample VC-12-05 only produced values up to 400 °C because,

above these temperature, all bending bars began to show internal fracturing and the mechanical excitation of the resonant frequency resulted in breakage of the sample.

Four-point bending tests and Weibull modulus

To investigate the samples' fracture behaviour after heat treatment, 10 (WK-silcrete samples) or 7 (VC-chert sample) bending bars of each sample, heated to the single temperature steps described above (for VC-12-05: 110 °C, 250 °C, 300 °C, 350 °C; WK-samples: 110 °C, 250 °C, 350 °C, 250 °C, 600 °C), were fractured in a four-point bending test (see for example Pais and Harvey 2012). Four supplementary bars were included in the measurements of WK-13-13 to increase the number of data spots (because the fracture position on some of the other bars was too far from the bar centre so that we were not confident about the measured values) and one measurement (WK-13-11 250 °C) did not produce valid data. E was not measured during these tests because the bending module's travel path could not be precisely recorded due to technical issues, and only fracture strength σ is reported here. This fracture strength value represents the maximum stress a bending bar withstands during the four-point bending test. The fracture stress value σ is calculated from the applied force and the geometric parameters of sample and rig (Munz and Fett 1989). However, the local stress is elevated at physical flaws and defects (microscopic notches, porosity, matrix-clast transitions) on the bar's tension side and their size, density and position vary from bar to bar. This also causes σ to vary from bending bar to bending bar within a single sample. Measurements of σ will consequently result in a distribution of values rather than a single value. This distribution is analysed using "Weibull plots" (i.e. double logarithmic diagrams plotting the maximum fracture strength on their abscissa against the probability of default on their ordinate, Weibull 1951). The Weibull modulus can be calculated from these plots. Samples that yield σ-measurements of high variation result in a low Weibull modulus, samples that show little variation from bending bar to bending bar have a higher Weibull modulus value. The modulus value is therefore a measure of the uniformity of a sample's fracture behaviour in terms of applied force at which fracture is initiated (in engineering, this is often termed the reliability of the material). The Weibull modulus is therefore a measure of the distribution of physical flaws and their sizes influencing the fracture behaviour of chert and silcrete before and after heat treatment.

Indentation fracture resistance

Indentation fracture resistance (IFR), a value closely related to fracture toughness (K_{Ic}) (Danzer et al. 2016), was measured by means of indentation for three samples: VC-12-05, Wk-13-08 and -13. During these tests, the length of surface cracks, propagating from the four apical points of an indentation, are measured to obtain a value related to the sample's real fracture toughness. As highlighted by Danzer et al. (2016), this method does not yield identical values of fracture toughness as determined by standard methods like single-edge notch-beam measurements. This is due to the effect of changes in stress distribution during the tests and therefore IFR has so far only been proven valid for silicon nitrides (ASTM F2094). However, due to the simplicity of the IFR procedure, it has been widely used and almost all of the available literature refers to "fracture toughness" as the number obtained from IFR. We continue here to use the notation K_{Ic} for our results, because it is a test which measures a resistance to crack extension, even though we have to caution against over-interpretation of the numeric values. As a number of ranking inside the IFR method on identical material, it is certainly a valid proxy for fracture toughness.

The experimental setup was as follows: separate bending bar fragments (resulting from the 110 °C four-point bending tests) were heat-treated with different temperatures (150 to 500 °C with 50 °C increments). K_{Ic} values after each heating step were averaged from 10 indentations placed on each fragment after cooling to room temperature. This protocol is justified by chert consisting of chalcedony (i.e. a non-oriented nano-crystalline quartz texture, Rios et al. 2001; Cady et al. 1998); thus, it can be expected that sample VC-12-05 behaves homogenously from sub-sample to sub-sample. Silcrete, however, consists of relatively large clasts in a finer-grained matrix and must consequently be expected to be more heterogeneous than chert. The experimental protocol for silcrete therefore aimed at minimising sample heterogeneity. For this, two diamond polished plates of WK-13-08 and -13 first received a row of 15 (WK-13-08) and 20 (WK-13-13) indentations that were measured and averaged. The plates were then heat-treated with a given temperature and received a second set of indentations after cooling to room temperature. After measuring these indentations, the plates were heat-treated at the next higher temperature (same temperatures as for VC-12-05 but up to 600 °C; except 150° for WK-13-13).

Quantitative fracture surface analysis

Previous studies have shown that chert and silcrete have different roughness or shininess of fracture surfaces produced before and after heat treatment (see for example Mourre et al. 2010; Schmidt et al. 2015; Tixier et al. 1980; Brown et al. 2009; Griffiths et al. 1987). The surfaces produced by fractures propagating through chert and silcrete were therefore quantitatively analysed using a laser scanning microscope (Keyence VK-X 130). This technique allows calculating common roughness parameters that characterise the fracture surface using the generated 3D-surface models. To perform these tests, a flake was removed from each sample before heat

treatment (by means of hard-hammer percussion with a granite cobble). The remaining pieces of the samples were heat-treated (with 300 °C for VC-12-05, based on the results of Milot et al. 2017; Schmidt et al. 2013a; and with 450 °C for the WK-sample, based on the results of Schmidt et al. 2015). After heating, another flake was removed and a 3D surface model was recorded on the ventral surface of each flake (unheated and heated) to compare the roughness parameters before and after heat treatment.

Instruments, settings and data treatment

Elastic modulus

Young's modulus was measured in flexural vibration mode at room temperature using an IMCE (Belgium) RFDA professional unit. The frequency range was 0–100 kHz. The calculation of E requires the dimensions and masses of the bending bard (as measured) and the material's Poisson's ratio (which we admitted to be equal to the one of silica glass: 0.17 cf. Tognana et al. 2010). The mechanical impulse was given by the unit's automated tapping device. Twenty-five measurements were recorded and averaged on each bending bar to account for possible heterogeneities within the bars: the fundamental flexural frequency was recorded 5 consecutive times at 5 different positions (two times near each tail end and one time in the middle) on each bending bar. Measurement errors for the stepwise heating sequence correspond to the dispersion of E in these 25 measurements. Errors of the single heating steps (Table 2; Fig. 2) correspond to the dispersion of E in all bending bars heated to a given temperature step.

Four-point bending tests and Weibull modulus

Bending tests were performed with a Kammrath & Weiss GmbH (Dortmund) bending module (MB2) according to the protocol specified DIN 51110: testing of advanced technical ceramics. During these tests, bending bars are placed into a bending module, the outer two bearing of which have a distance of 30 mm (tension side) and the inner two of 15 mm, with their two chamfered edges at the face stressed in tension. The bars were pre-loaded with 10 N. The four-point bending test began after 30 s of preloading time, by applying a constant load speed of 0.18 mm/min until failure of the bending bar (only bending bars that broke between the two inner bearings were recorded as valid). The fracture strength σ is calculated from the maximum force at failure in the usual way (Munz and Fett 1989). Errors of the average values of σ of a given temperature step (Table 3) correspond to the dispersion of σ as measured in all bending bars heated to this temperature.

Indentation fracture resistance

The average K_{Ic} value of the samples after different heating steps was measured by indentation with a Vickers diamond. The applied load was 100 N (using a DOLI universal test machine) and hold time of the load for 30 s. K_{Ic} was then calculated from the length of the surface cracks that develop from the four apical points of each indentation, using the mathematical model for half-penny shaped cracks given in Niihara et al. (1982). Resolving this formula for K_{Ic} requires the length of the

Table 2 Results of the RFDA measurements of the elastic modulus (E *[GPa]*) in silcrete and chert samples. Values in the column "Step HT" are the values of the stepwise heating sequence of a single bending bar. Errors of these values correspond to the rage of values obtained from 25 measurements of every bending bar. Values in the column "HT" are the values of the single heating experiments (the number of bending bars that produced this average value and its error range in brackets)

	VC-12-05		WK-13-08		WK-13-11		WK-13-13	
Temp. [°C]	Step HT	HT	Step HT	HT	Step HT	HT	Step HT	HT
110	75.19 ± 0.03	74.89 ± 3.09 (35)	71.32 ± 0.04	67.42 ± 15.55 (49)	89.44 ± 0.04	81.79 ± 13.1 (48)	80.9 ± 0.01	76.41 ± 11.3 (53)
150	75.61 ± 0.01		71.43 ± 0.04		89.48 ± 0.02		80.37 ± 0.01	
200	75.76 ± 0.01		71.13 ± 0.03		89.14 ± 0.02		79.39 ± 0.06	
250	75.89 ± 0.03	75.89 ± 1.39 (6)	70.61 ± 0.04	64.6 ± 12.47 (10)	88.85 ± 0.03	80.9 ± 11.16 (10)	77.86 ± 0.17	75.57 ± 6.56 (10)
300	75.93 ± 0.01	76.33 ± 2.46 (7)	70.01 ± 0.05		88.28 ± 0.04		74.20 ± 0.54	
350	76.2 ± 0.01	76.37 ± 1.64 (7)	69.7 ± 0.04	63.98 ± 18.61 (10)	86.95 ± 0.09	76.62 ± 18.49 (10)	69.37 ± 0.58	68.43 ± 6.75 (10)
400	76.47 ± 0.01		69.49 ± 0.04		85.37 ± 0.1		63.99 ± 2.23	
450			69.22 ± 0.05	63.83 ± 12.52 (10)	82.99 ± 0.09	70.27 ± 10.93 (10)	61.05 ± 3.01	60.3 ± 9.87 (10)
500			68.68 ± 0.06		80.56 ± 0.12		59.70 ± 0.88	
550			67.50 ± 0.12		76.36 ± 0.16		56.43 ± 2	
600			62.33 ± 0.25	58.86 ± 14.77 (9)	68.47 ± 0.2	56.69 ± 14.38 (9)	46.73 ± 1.29	48.65 ± 12.41 (10)

Table 3 Results of the fracture strength σ [MPa] measurements obtained from bending tests. Means are calculated from all bending bars heated to a single temperature step. Errors of these means are standard deviations calculated from the scattering of these values. σ_c = characteristic strength as defined by Weibull (1951) taken from the abscissa intersection in the Weibull plots

	VC-12-05					WK-13-08				
Temp. [°C]	110	250	300	350		110	250	350	450	600
fracture strength [N/mm^2]	65.92	63.86	101.68	102.36		34.7	38.56	27.46	44.02	36.52
	171.44	141.51	132.56	115.63		35.31	39.45	41.96	49.23	40.7
	173.58	154.32	148.57	124.34		51.84	41.53	55.32	50.96	48.64
	174.29	156.47	149.2	140.95		53.62	42.75	57.28	55.7	52.41
	175.99	165.44	153.61	147.61		54.19	46.02	60.38	56.3	52.72
	191.43	192.44	183.87	149.68		54.63	49.73	62.87	57.17	57.19
	213.06	206.2	213.85	155.08		55.33	54.98	64.24	58.83	59.02
						61.04	62.85	70.43	69.95	62.78
						66.26	66.01	73.81	70.57	66.14
						67.25	66.26	84.38	73.97	72.86
Mean:	166.53	154.32	154.76	133.66		53.42	50.81	59.82	58.67	54.9
Error:	± 21.7	± 21.2	± 16.6	± 9.2		± 5.2	± 5.2	± 7.6	± 4.7	± 5.3
	WK-13-11					WK-13-13				
Temp [°C]	110	250	350	450	600	110	250	350	450	600
fracture strength [N/mm^2]	15.48	15.59	24.58	30.48	23.81	16.78				24.89
	16.01	23.3	25.7	30.49	27.17	17.67	30.31	29.07	24.9	25.78
	26.62	25.02	33.49	31.7	29.84	21.25	33.2	29.85	29.17	28.12
	27.33	31.43	34.26	34.59	31.06	24.45	33.71	33.39	30.16	29.45
	28.22	33.99	35.01	36.01	31.97	31.16	35.67	34.85	30.25	29.78
	32.84	34.64	38.12	37.52	37.9	33.82	38.29	35.55	32.94	31.35
	33.13	34.73	39.2	38.72	38.12	39.34	43.33	38.19	33.31	32.23
	34.64	37.97	40.97	41.65	39.24	41.53	43.75	39.9	34.53	33.77
	40.12	41.71	42.38	44.73	39.44	42.97	43.84	40.05	36.06	34.02
	48.62		46.02	45	42.87	44.13	43.95	40.34	37.11	35.47
						45.61	53.15	45.82	38.61	36.75
						45.8				
						67.37				
Mean:	30.3	30.93	35.97	37.09	34.14	36.3	39.92	36.7	32.7	31.06
Error:	± 4.8	± 3.8	± 3.3	± 2.6	± 3.0	± 6.8	± 3.3	± 2.5	± 2.0	± 1.8

surface cracks, the diagonal of the indentation, the material's Vickers hardness (VH) and Young's modulus (*E*). Crack length was directly measured using a scanning electron microscope (HITACHI Tabletop Microscope TM3030 Plus); *E* was taken from the RFDA measurements of the bending bars heated to the corresponding temperatures (because *E* values for the chert sample VC-12-05 were only available up to 400 °C, the modulus value recorded at 400 °C was also admitted for the two K_{Ic} measurements at 450 °C and 500 °C). VH values could not be calculated from most of the indentations because their margins flaked off at a load of 100 N, making precise VH measurement impossible. We therefore admitted a standard value of quartz (11.65 GPa) and calculated the theoretical diagonal left at 100 N by a Vickers pyramid in a material with this hardness to be 126 μm. The few indentations with intact margins, where the indentation diagonal could be measured, confirmed that the value used is a fair approximation for the material at hand. The K_{Ic} value of an indentation was averaged from its four cracks. The K_{Ic} value at a given temperature step was averaged from all indentations in the set. Error bars are standard deviations calculated from all indentations within the set.

Quantitative fracture surface analysis

3D surface models were recorded with a Keyence VK-X100 laser scanning microscope. Measurements on chert were made with a 50× objective, silcrete measurements were made with a 20× objective. In both cases, nine tiles were recorded and stitched together to obtain a field of view of 1923 μm × 1400 μm for silcrete and 750 μm × 500 μm for chert. 3D models are shown as overlay of height data and the real image of the surface. We report the roughness parameters R_a (the so-called roughness average) and R_z (the ten-point mean profile depths). R_a is the mean height of all peaks and valleys as measured from the mean value of all heights. As such, the value expresses the overall surface roughness, taking into account small and high peaks and for statistical reasons largely disregarding rare extremes; R_z is the average distance between the highest peak and lowest valley (a value expressing the maximum profile depth of the surface). Both R_a and R_z were calculated from all pixels in the whole array of the 3D models (all 9 tiles), hence are statistically more robust than traditional 1D profile measurements. Before roughness analysis, the 3D models were corrected for surface inclination with a circular fit. R_a and R_z values are reported from primary profiles,

without cut-off filtering (these are representative of a mixture of roughness and waviness), and after applying a cut-off filter (high-pass filter λ_c) of 0.08 mm (representative of the high frequency surface roughness). We tried to add a supplementary low-pass filter (λ_s) to eliminate possible small-scale noise in the 3D models but found no significant difference (≤ second decimal place) with values obtained without a low-pass filter.

Results

Elastic modulus

Values of *E* obtained during the stepwise heating sequence of chert and silcrete samples are summarised in Table 2 and graphically shown in Fig. 1. The chert sample VC-12-05 shows a small but significant increase in elastic modulus after heat treatment. After heating to 400 °C, its *E* value is increased by 1.7%. The tree WK-silcrete samples document the inverse trend by showing a clear decrease of *E* with rising temperatures. While the differences between the initial *E* values of the three silcrete values are not significant (initial *E* values measured in different bending bars of a single sample vary up to ± 15 GPa, cf. Table 2), a clear trend can be noted in the magnitude of loss. WK-13-08 loses ~ 14% of its initial *E* value after heating to 600 °C, WK-13-11 loses ~ 23% and WK-13-13 loses ~ 45%. Figure 2 shows *E* values obtained by heating of different bending bar sets to single temperature steps, as compared with the stepwise heating sequences. Single heating *E* values of the chert sample VC-12-05 plot slightly above the values obtained from the heating sequence. In silcrete samples, all mean *E* values obtained by single heating (except one: WK-13-13 at 250 °C) yielded results comparable with the stepwise heating sequences within the measured error. These data document that stepwise heating is representative of single heating steps for silcrete and produces reasonably close values for chert. The following discussion of the causes of the thermal induced changes of *E* will therefore only take into account the results from the stepwise heating sequence.

Four-point bending tests and Weibull modulus

Fracture strength values obtained during the four-point bending tests of chert and silcrete samples are summarised in Table 3 and graphically shown in Fig. 3a, b. Initial σ values are significantly different in chert and silcrete. Chert sample yielded a value of 166 ± 22 N/mm^2, while silcrete samples have values in the range of ~ 30 to ~ 50 MPa (Table 3). The 350 °C measurements of chert sample VC-12-05 resulted in a significantly lower σ. None of the silcrete samples show strong changes in σ upon heating, although a trend of decreasing σ may be interpreted from samples of WK-13-13. An example of a Weibull plot is shown in Fig. 3c; values of the Weibull modulus of the four samples after

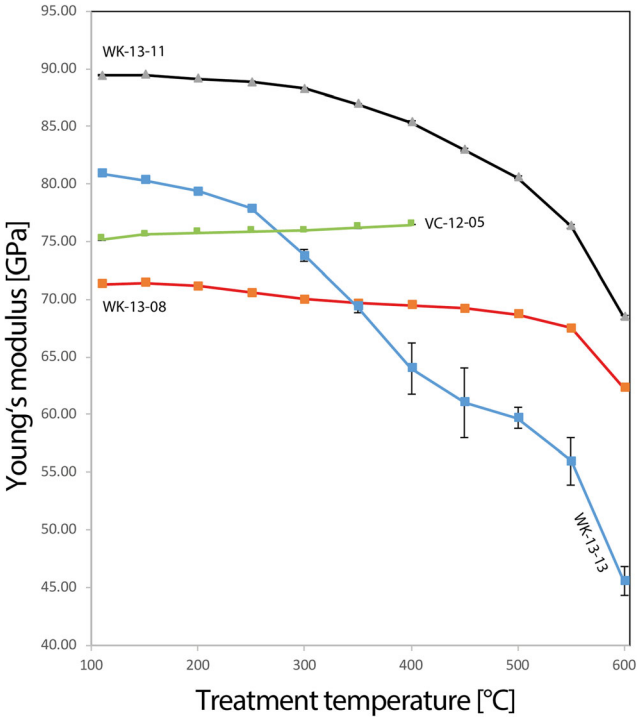

Fig. 1 Thermal evolution of Young's modulus (*E*) in silcrete and chert samples in GPa. The initial magnitude of *E*, before heating, is not representative of the samples. *E* values measured in different bending bars vary up to ± 15 GPa in a single sample (Table 2). Only the magnitude of the modulus loss/gain and its progression with rising temperature are significant. Note that the chert sample VC-12-05 shows the inverse trend

heating to different temperatures are summarised in Table 4 and graphically shown in Fig. 4. Except for the 350 °C measurements of sample WK-13-08, heat treatment resulted in an increase of the Weibull modulus in all samples. For silcrete sample WK-13-13, the onset of this Weibull modulus gain lies between 110 and 250 °C; for WK-13-11 and the chert sample VC-12-05 between 250 and 350 °C. Thus, all samples perform more homogeneously with regards to their fracture behaviour after heat treatment.

Indentation fracture resistance

K_{Ic} values obtained from indentation testing of silcrete and chert samples are shown in Fig. 5a–c. All three samples show similar initial K_{Ic} values near 1.8 MPa m$^{1/2}$, indicating that IFR alone does not allow to differentiate between chert and silcrete. K_{Ic} in the chert sample VC-12-05 did not significantly change until 200 °C but began to decrease from this temperature onwards. This trend is probably continuous over the whole temperature range. The initial K_{Ic} value is lowered by the heat treatment to approximately 1/3. The two analysed silcrete samples WK-13-08 and -13 show very similar trends up to a treatment temperature of 300–350 °C, only the errors are larger. No significant change is observed up to 200 °C,

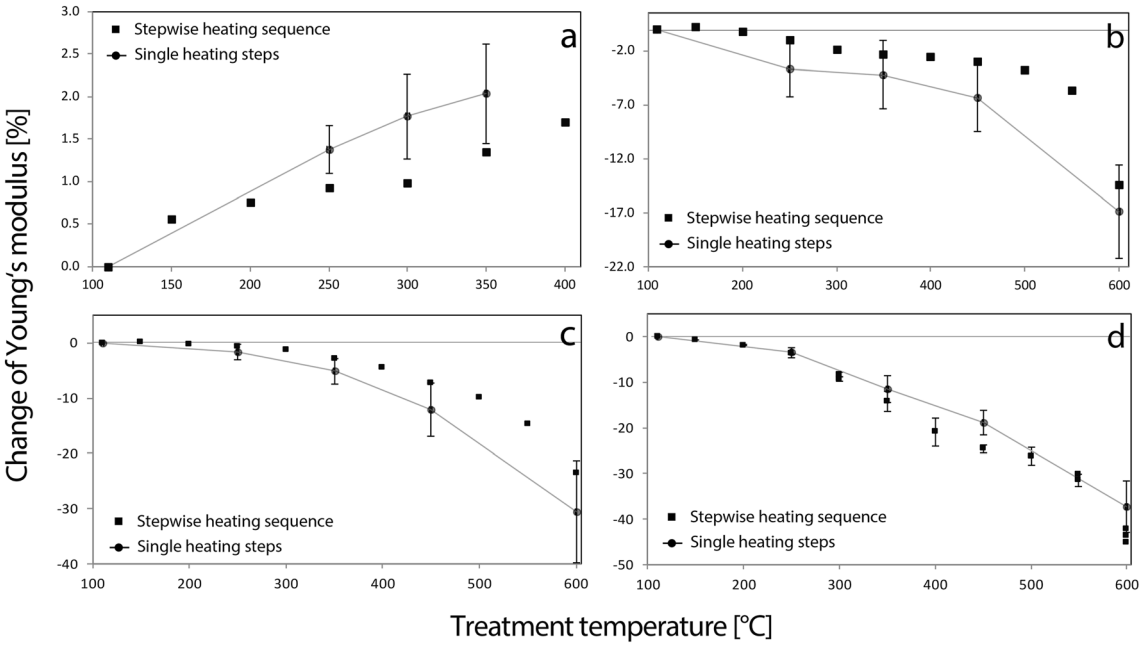

Fig. 2 Comparison between the thermal evolution of Young's modulus measured during stepwise heating and single heating to the same temperatures. **a** VC-12-04, **b** WK-13-08, **c** WK-13-11 and **d** WK-13-13. For comparability between both heating series, values are plotted in percent change. Error bars for single heating data are the scattering of values recorded on different bending bars. Note that almost all single heating and stepwise heating produced the sample results within the measured error

above which K_{Ic} is steadily lowered till 300–350 °C. At higher temperatures of treatment, a rather constant level near 1.3 MPa √m is indicated. The differences between chert and silcrete are thus the continuation of the lowering of the K_{Ic} level with increasing temperature of treatment in chert beyond 350 °C, which leads to a much lower level in chert.

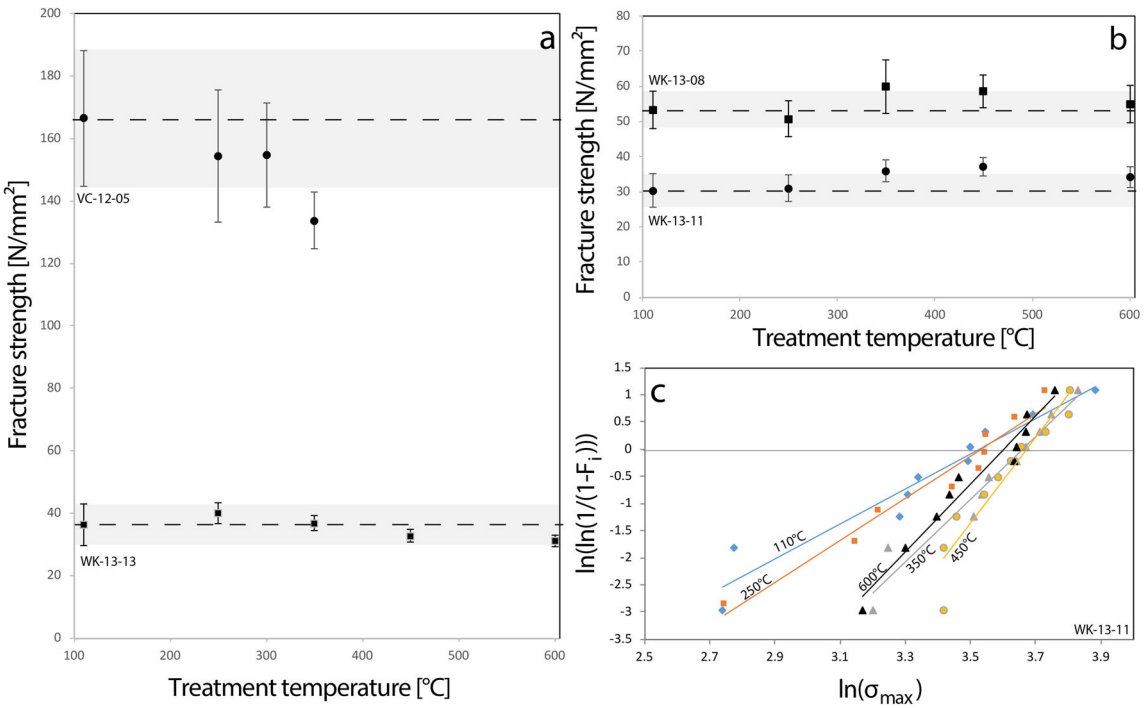

Fig. 3 Thermal evolution of fracture strength in silcrete and chert (**a**, **b**) and one example of a Weibull plot (**c**), plotting the fracture strength values of silcrete sample WK-13-11. **a** and **b** are separated for better readability of the data. Note that except for the 450 °C measurements of WK-13-11 and the 350 °C measurements of VC-12-05, the changes in fracture strength are not significant. A trend of increasing fracture strength with rising temperature can, however, be noted for two of the silcrete samples. The chert sample shows the inverse trend. In Weibull plots, the slope of the linear best fit is the dimensionless Weibull modulus

Table 4 Weibull modulus of the silcrete and chert samples as calculated from the fracture strength values in Table 3

Temp. [°C]	VC-12-05	WK-13-08	WK-13-11	WK-13-13
110	2.61	5.01	3.23	2.85
250	2.87	5.28	3.89	6.76
300	4.97			
350	7.61	3.72	5.81	8.31
450		6.96	7.85	9.19
600		5.67	6.28	9.52

These silcrete IFR values and their thermal evolutions are representative of the bulk rocks (Fig. 5b, c) because the measured cracks ran through clasts and matrix regardless. However, during indentation testing of silcrete sample WK-13-13, it was possible to separate out K_{Ic} measurements of the quartz clast only: indentations of up to 1-mm large clasts (cf. Table 1) had cracks, which did not exceed the clast margins, i.e. the measured value corresponds to the quartz clast only. These values are reported as a separate sequence in Fig. 5d. The initial K_{Ic} value of these clasts before and after heating is near 1.3 MPa $m^{1/2}$; hence, the clasts do not change in their fracture toughness after heat treatment and the level of their fracture toughness coincides with the plateau values of silcrete after heating above 350 °C (Table 5).

Quantitative fracture surface analysis

3D surface models of fracture surfaces, before and after heat treatment, are shown in Fig. 6 and roughness values calculated from the models are summarised in Table 6. The initial roughness of fracture surfaces on chert and silcrete is different before heat treatment with the surface of chert samples VC-12-05 being more than 20 times smoother than the average surface of the three silcrete samples.

If no cut-off filter is applied (i.e. primary profile R_a, representing a mixture of roughness and waviness of the surface), the R_a value of chert sample VC-12-05 is reduced by 26% after heat treatment, and the ten-point mean profile depth R_z by 44%. In silcrete, R_a is reduced by 57%, 34% and 20% in WK-13-08, -11 and -13, respectively. Ten-point mean profile depth is reduced in silcrete by 4%, 16% and 27% (WK-13-08, -11 and -13 respectively). A similar trend can be observed in real R_a values, if a 0.08 mm cut-off filter is applied: mean roughness is reduced after heat treatment, although the percentages are slightly different (Table 6).

Thus, in both silcrete and chert, there is a decrease in R_a. The relative change is stronger in chert. The R_z values, highlighting the maximum values from the profiles, are also reduced in chert and silcrete.

Discussion

A critical review of RFDA, fracture strength and indentation data

The absolute *E* values obtained by our RFDA measurements do show little variation within single samples, which indicates a good repeatability and point towards a high accuracy of measurement. The variations of up to ± 15 GPa within a set of 50 bending bars, cut from a single block of silcrete, are easily understood from the structural heterogeneity of silcrete, which should be seen as a composite of larger clasts with a fine matrix, in which both the relative amount and the clast sizes vary strongly. Nonetheless, both chert and silcrete are mainly composed of α-quartz and therefore are expected to have a similar Young's modulus, which they do before any heating is done. The change in Young's modulus with temperature of treatment is strongly different between chert and silcrete. Chert increases in *E*, at least when treated above

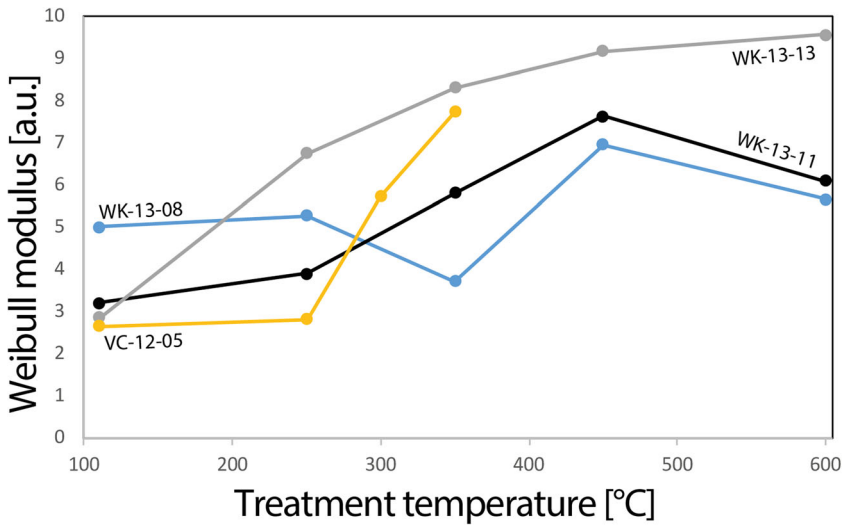

Fig. 4 Thermal evolution of the Weibull modulus of chert and silcrete samples. Measurements for the three silcrete samples were made at 110, 250, 350, 450 and 600 °C; measurements for chert were made after heating to 110, 250, 300 and 350 °C

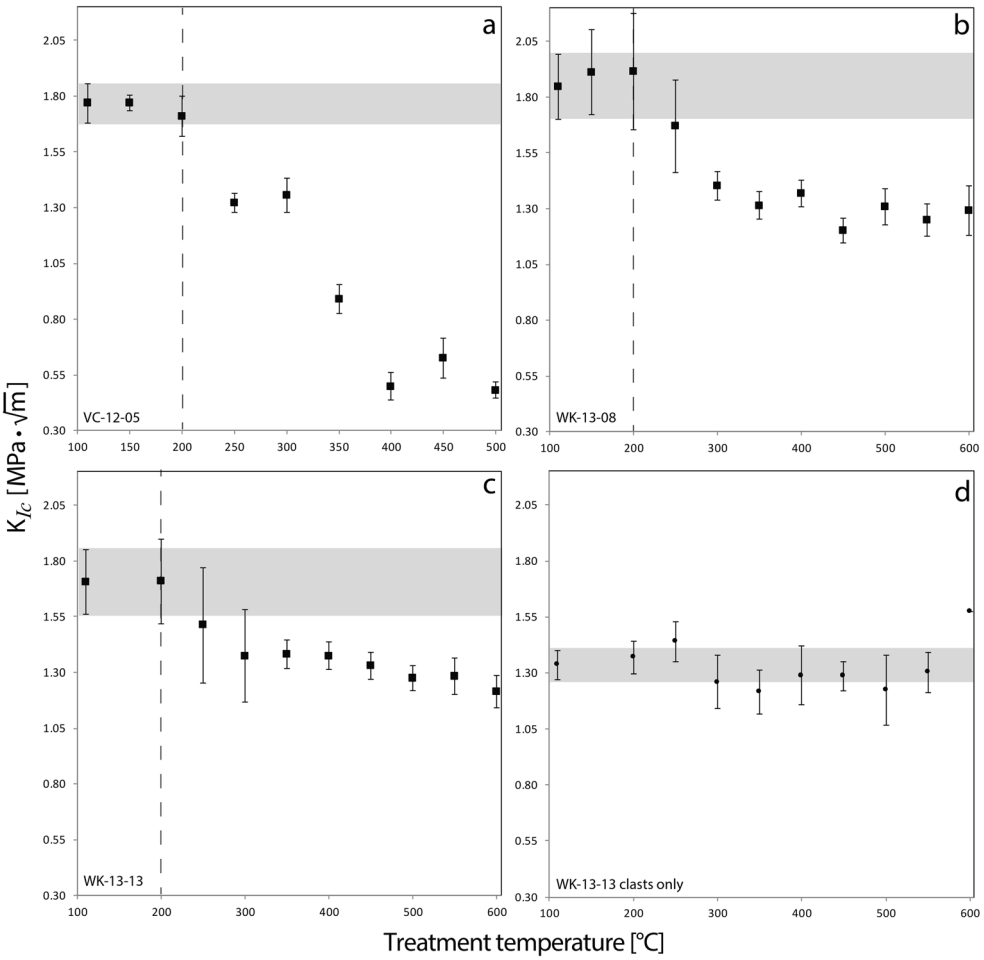

Fig. 5 Thermal evolution of the average indentation fracture resistance (K_{Ic}) value of chert sample VC-12-05 (**a**) and silcrete samples WK-13-08 (**b**) and WK-13-13 (**c**). **d** A plot of K_{Ic} recorded in quartz clasts embedded in sample WK-13-13 (no matrix taken into account). Note that in all three samples, K_{Ic} begins to drop from 200 °C onwards. Error ranges of the unheated sample measurements are marked by grey bars across the plots to graphically evaluate the significance of the K_{Ic} loss. In WK-13-13 (**c**), values after heat treatment to temperatures above 350 °C approach the K_{Ic} values of the quartz clasts in this sample

200 °C, on a low but very well defined level. Silcretes show a strong loss in Young's modulus with treatment temperature, but the trend is neither similar between the silcrete types nor described by a simple monotonic trend. There is an indication that silcretes with more clasts are lowered more strongly in E compared to finer silcrete. This points to structural changes (development of matrix/clast microcracks, secondary void creation by shrinking of accessory minerals or similar processes) to be responsible here. Further investigations are necessary to clarify the picture.

A different picture emerges from the fracture strength data. The comparison between the absolute values of chert and silcrete illustrates differences between the fracture behaviours of both material classes (chert has higher fracture strength by a factor of 3). According to Griffith's (1921) theory of fracture mechanics, this difference can only be explained by much

Table 5 Indentation fracture resistance (K_{Ic}) of chert and silcrete samples in MPa $m^{1/2}$

Temp. [°C]	K_{Ic} of VC-12-05	K_{Ic} of WK-13-08	K_{Ic} of WK-13-13	K_{Ic} of WK-13-13 clasts
110	1.77 ± 0.09	1.85 ± 0.14	1.71 ± 0.19	1.34 ± 0.06
150	1.77 ± 0.03	1.91 ± 0.19	–	–
200	1.71 ± 0.09	1.92 ± 0.26	1.71 ± 0.14	1.37 ± 0.07
250	1.32 ± 0.04	1.67 ± 0.21	1.51 ± 0.12	1.44 ± 0.09
300	1.36 ± 0.08	1.4 ± 0.06	1.37 ± 0.11	1.26 ± 0.12
350	0.89 ± 0.06	1.31 ± 0.06	1.38 ± 0.12	1.22 ± 0.1
400	0.5 ± 0.06	1.37 ± 0.06	1.37 ± 0.1 -	1.29 ± 0.13
450	0.63 ± 0.09	1.2 ± 0.06	1.33 ± 0.09	1.29 ± 0.07
500	0.48 ± 0.04	1.31 ± 0.08	1.27 ± 0.09	1.22 ± 0.16
550	–	1.25 ± 0.07	1.28 ± 0.11	1.3 ± 0.09
600	–	1.29 ± 0.11	1.22 ± 0.09	1.57 ± 0

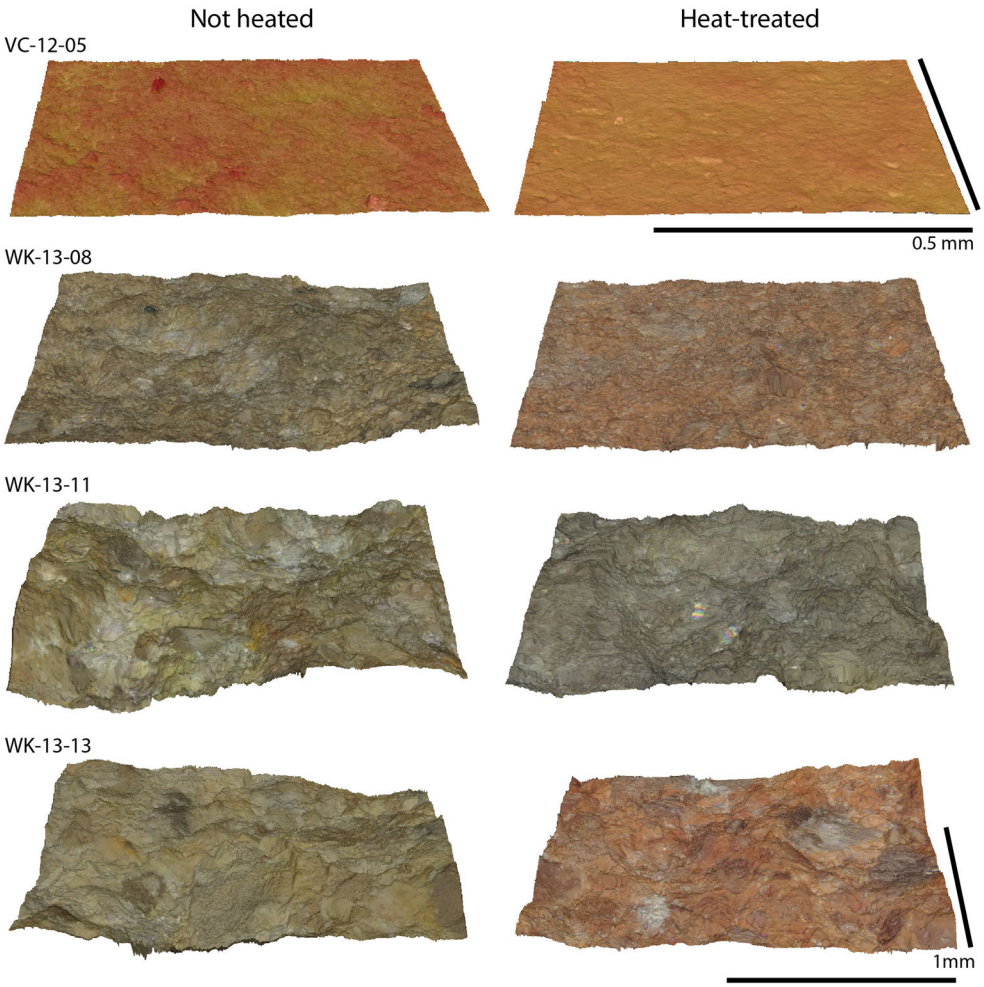

Fig. 6 3D surface models of fresh fracture scars on chert and silcrete sample before (left) and after (right) heat treatment recorded by a laser scanning microscope. Note that fracture scars post-dating heat treatment are noticeably smother than before heat treatment. Roughness values obtained from these surface models are summarised in Table 6

smaller flaws being present in the very fine grained rocks. Nonetheless, these flaws have to show a considerable natural variation in size, which is indicated by the fairly low Weibull modulus. Heating above 200° may be interpreted to lower the average fracture strength of the tested chert sample but measurement errors are too large to make definitive statements based on our data on fracture strength.

In the unheated state, our study did not show major differences in E or K_{Ic} between chert and silcrete. This comes as a surprise because chert is considered by many archaeologists (see for example Marean 2015) a raw material of far better quality for stone tool knapping than silcrete. Thus, neither E nor K_{Ic} can be used alone to characterise the knapping quality of silica rocks, opening up new questions about the adequacy

Table 6 Roughness parameters R_a and R_z as obtained from 3D surface models of fresh fracture surfaces before and after heat treatment. Values under ΔR_a and ΔR_z are the relative change from unheated to heat-treated in percent

		No cut-off filter				0.08 mm cut-off filter			
	Temp. [°C]	R_a [µm]	R_z [µm]	ΔR_a	ΔR_z	R_a [µm]	R_z [µm]	ΔR_a	ΔR_z
VC-12-05	Unheated	1.498	24.827	− 26%	− 44%	0.8	18.979	− 47%	− 44%
	300	1.102	13.951			0.423	10.58		
WK-13-08	Unheated	21.882	427.478	− 57%	− 4%	6.715	404.985	− 32%	− 2%
	450	9.515	410.721			4.546	397.955		
WK-13-11	Unheated	40.82	423.353	− 34%	− 16%	10.336	424.415	− 16%	− 6%
	450	26.861	354.606			8.696	400.482		
WK-13-13	Unheated	30.378	547.739	− 20%	− 27%	9.178	366.368	− 22%	+ 10%
	450	24.152	401.426			7.148	401.905		

of specific mechanical testing methods for investigating questions related to archaeology and stone tools making.

Our Weibull data should be considered with some caution. The number of tested bending bars that led to estimate Weibull modulus values is rather low as compared to the recommended number of data points used for this method (Weibull 1951). The data from the treatments at 600 °C should not be over-interpreted here, because at those temperatures we induce the α/β-quartz transition, which can be expected to be responsible for a flaw population. The comparison between absolute Weibull modulus values in different samples must therefore be regarded as indication only and further experiments are recommended.

The secure assertions stemming from our results are: [1] the main difference between chert and silcrete is their fracture strength. Their fracture resistance, consistency of their fracture behaviour (as documented by their Weibull modulus) and their elastic properties cannot be used to distinguish both material classes in an unheated state. [2] Upon heating, both materials experience a significant drop of K_{Ic} and [3] an increase of their Weibull modulus, i.e. fracture propagation is facilitated and they behave more uniformly during fracturing. [4] The fracture surfaces of both materials are measurably smoother after heat treatment, indicating that during post-heat treatment knapping, fractures propagating through the material are less offset from an ideal conchoidal path. [5] The loss of K_{Ic} is two to three times stronger in chert than in silcrete. [6] The elastic properties of both materials show inverse trends.

The chemical and crystallographic origin of the changes in mechanical properties

Combining our results with previously published data on chert and silcrete, it is possible to shed light on the chemical origins of the changes in mechanical properties of chert and silcrete. Detailed data on the temperature-induced loss of chemically bound water is available for all three silcrete samples from Schmidt et al. (2017a). SiOH data of a sample coming from the same outcrop as our chert sample VC-12-05 is available from an unpublished series produced during the experiments detailed in Schmidt et al. (2013a). Although the results section of this publication only included data on the loss of porosity and the bonding behaviour of surface silanol in this sample, the experiment that produced these data also yielded quantitative data on the loss of SiOH. These unpublished data of Schmidt et al. (2013a) is provided in the present study (the experimental and instrumental setup used for data collection is detailed in the original publication).

Both these sets of SiOH data, of chert and silcrete, are summarised in Fig. 7a. Comparing these SiOH data with our K_{Ic} data (as summarised in Fig. 7b), it can be noted that both data sets show a plateau at low temperatures, indicating that SiOH loss and K_{Ic} drop both require a minimum heating temperature of > 200 °C for their onset. The drop in K_{Ic} with treatment temperature is rather similar for both silcrete and chert in the range 200–350 °C. As pointed out before, the presence of quartz clasts in silcrete seems to prevent a drop below the value for these clasts (Fig. 7b).

The correlation plot of *c* SiOH vs. K_{Ic} in Fig. 7c gives insight into one detail of the process: the loss of chemically bound water in silcrete and chert is connected to, and hence may be responsible for, the changes of IFR.

Another way of verifying this correlation is by comparing the magnitudes of loss of different variables. Figure 7d is a plot comparing the losses of SiOH, real and primary profile R_a, K_{Ic} and *E* (always from unheated to the highest measured heating temperature). It can be followed from this plot that samples containing a larger amount of matrix (finer-grained samples) lose more SiOH and accordingly the K_{Ic} and R_a losses are also stronger. Coarser-grained samples initially contain less SiOH and the 'water'-loss upon heating is less pronounced. In these samples, the thermally induced changes of K_{Ic} and R_a are also less intense. This relation can be explained by the theory of thermal transformations occurring in chert (Schmidt et al. 2011, 2012b) and silcrete (Schmidt et al. 2013b, 2017a). In both types of rock, SiOH loss is followed by the formation of new Si–O–Si bonds at internal surfaces and pore walls. This leads to a measurable domain size increase of the rock's quartz nano-crystals (Dejoie et al. 2015) and may effectively close and reduce narrow flaws and defects in the bulk material. This way, a partial closure would lead to a diminishing of the intergranular pore space and decrease the flaw size. While this may explain a more homogeneous fracture behaviour, it would have a tendency to increase strength. However, this is counterbalanced by the lowering of the K_{Ic}. Internal healing of crack-like defects with silanol covered surfaces would eradicate the—probably randomly oriented—pathways, which deter a running crack from the ideal path in the stress field applied. Therefore, the overall crack path length is decreased towards a straighter, shorter crack path, which has a lower amount of energy. In other words, the internal defects of the original material—either as microcracks or at grain boundaries—acted as toughening mechanism. In engineering, these effects would be crack deflection, crack branching, microcracking and potentially an R-curve effect (Wachtman et al. 2009). In this way, we may explain the increased K_{Ic} of chert and silcrete (in the order of 2 MPa √m) compared to the clast values at 1.3 MPa √m and the ultra-low values of chert heated to high temperatures.

A difference between chert and silcrete is the shape and size of the pore space, which is in silcrete up to 5 times larger than in chert (compare Schmidt et al. 2013a, 2017a). The thermal processes discussed above may not be sufficient to close larger voids in silcrete (Schmidt et al. 2017a). Unaltered macropores may therefore account for the unaltered strength in silcrete but the closure of finer intergranular pores through grain bridging causes the observed loss of toughness.

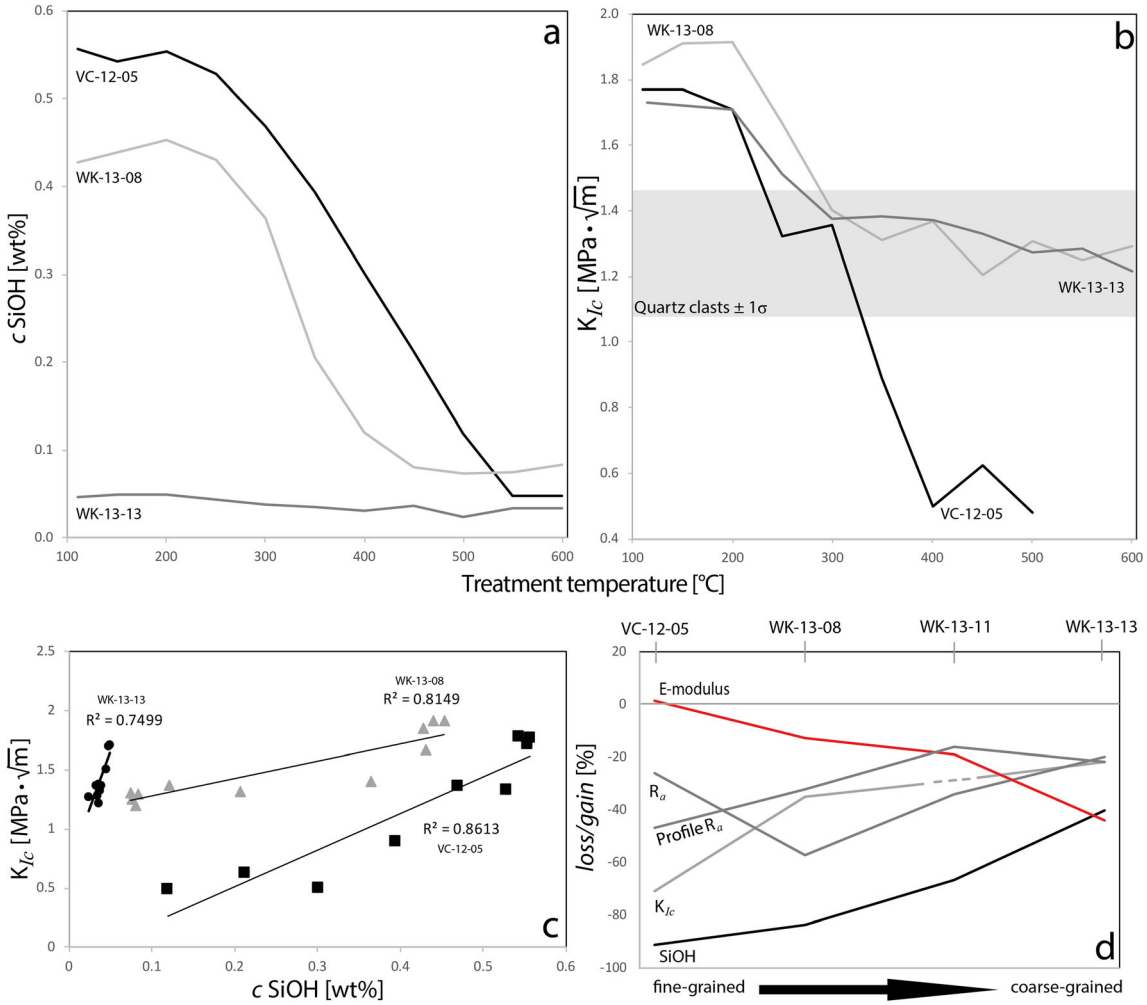

Fig. 7 Overview of the thermally induced changes in fracture resistance (K_{Ic}), E-modulus, fracture surface roughness (R_a) and loss of chemically bound water (SiOH) in chert and silcrete samples. **a** Concentration *c* of SiOH: silcrete data from Schmidt et al. (2017a); chert data from an unpublished series produced during the experiments in Schmidt et al. (2013a). **b** Overview plot of the K_{Ic} data of the three samples for which SiOH data is plotted in **a**. The grey bar marks the range (within 1 standard deviation) of K_{Ic} data measured from quartz clasts over all temperatures. **c** Correlation plot of K_{Ic} over *c* SiOH at different heating temperatures as extracted from **a** and **b**. **d** Plot comparing the loss/gain of SiOH, K_{Ic}, R_a, primary profile R_a and E-modulus in percent as calculated from **a**, **b** and Tables 2 and 6. In **d**, samples are ordered from left to right, representing the finest-grained to the coarsest-grained sample. Note that samples that loose larger quantities of SiOH during heating show stronger decrease in their K_{Ic} and R_a values; the inverse trend is observed for their E modulus (**d**). Also note that the progression of the temperature induced K_{Ic} loss shows a reasonably good correlation with SiOH loss in the samples (**c**)

Defect healing can also be expected to increase the stiffness of the rocks, as expressed by increasing *E* after heating (see for example Angel et al. 2009). The increase of *E* in chert sample VC-12-05 can thus be explained by the formation of new Si–O–Si bonds in chalcedony (Schmidt et al. 2011, 2012b). However, *E* in silcrete does the opposite as in chert: it drops after heat treatment. Comparing the three silcrete samples, it can also be noted that it is in opposition to the evolution of K_{Ic} and R_a (Fig. 7d), indicating that there is no straightforward correlation with SiOH loss as for the other parameters.

We did not expect this because the same mechanism of Si–O–Si formation upon SiOH loss takes place in silcrete (Schmidt et al. 2013b, 2017a). Internal micro-fracturing in silcrete can be ruled out as possible cause because it was shown to onset at higher temperatures than the reduction of *E* (Schmidt et al. 2017a). Another possible explanation would be the creation of voids (see for example (Asmani et al. 2001)) due to heat-induced processes associated with non-quartz impurities (shirking, sintering, etc.). Indeed, South African silcrete is not pure quartz but was found to contain up to a few weight percent of impurities, mainly TiO_2, Fe_2O_3 and Al_2O_3 (Roberts 2003). These are for example present as anatase, iron oxides and clay (Summerfield 1983; Schmidt et al. 2013b, 2017a). A strong reduction of stiffness due to the opening of voids could be expected to mask the weaker processes associated with the creation of new Si–O–Si bonds in silcrete. Whether this explanation is worthy of further investigation can only be decided after systematic studies on the thermal transformations of non-

quartz components in silcrete. As it stands, our study can only explain the structural origins of heat-induced changes of K_{Ic}, R_a of fresh fracture scars and Weibull modulus. The thermal evolution of stiffness in chert can be satisfactorily explained but it remains unclear in silcrete.

Comparison with previously published data

These data allow to confirm and refine several previous studies on the heat treatment effects of silica rocks while refuting others. For example, the lack of thermal evolution in our fracture strength measurements is in contradiction with Purdy and Brooks (1971) who had found a 25–40% increase of compressive strength and a 45% reduction of tensile strength in chert from Florida. These differences might be due to dissimilar measuring protocols (this cannot be evaluated because of the lack of detail in their publication) or different composition of the analysed samples. Heating of sample VC-12-05 to 350 °C did result in a weak loss of strength but we rather attribute this to the onset of internal fracturing in this type of chert (Schmidt et al. 2013a), than to the same thermal processes that cause the K_{Ic} drop (internal fractures were macroscopically observed after heating to 350 °C). The loss of toughness (IFR) we observed during our experiments largely corroborates the results of Schindler et al. (1982) who had found a temperature-dependant K_{Ic} curve (also indentation data) with similar shape for chert as we did (showing a plateau at the lower range of used heating temperatures that indicates a similar minimum activation temperature for the onset of the reaction).

Our data also corroborate more experimental studies on knapping quality that had pointed out an increased ease of flake detachment from heated chert (Sollberger and Hester 1973) and better quality for pressure flaking or free hand knapping (see among many others Inizan et al. 1976; Griffiths et al. 1987). It was also quantitatively shown that flakes removed from heated chert are longer than their unheated counterparts (Bleed and Meier 1980). All these observations can be satisfactorily explained by the loss of resistance to fracture propagation (toughness) after heat treatment.

Another study (Domanski et al. 1994) on the mechanical properties of different silica rocks also highlighted the importance of fracture toughness during heat treatment. This study presents the by far most detailed dataset produced on more than 20 samples of chert, hydrothermal chalcedony, quartzite, obsidian and silcrete. Unfortunately, the high number of samples and tests (4 mechanical properties) precluded measurements at temperatures < 300 °C and sufficiently narrow-spaced temperature steps, so that it is difficult to evaluate the interdependence of different variables or their correlation with our data. It is, however, possible to compare their absolute fracture toughness values with our indentation resistance values. Fracture toughness of chert (there also called flint) was found to range between 1.5 and 2.5 MPa $m^{1/2}$, most of the samples being close to 1.6 MPa $m^{1/2}$, thus reasonably close to our values. Fracture toughness of silcrete was found to range from 1.8 to 2.5 MPa $m^{1/2}$. The lower range of these values, obtained by short rod fracture toughness testing, is in good agreement with our data obtained by Vickers indentation.

Another sometimes misunderstood aspect in the study of rock heat treatment is the role of the quartz α to β phase transition. Wadley and Prinsloo (2014) suggested that the gloss in fresh fracture scars of silcrete knapped after heating was an indication that the quartz inversion played a major role during heat treatment (*op. cit.,* p. 57). They even claimed that heat-treated silcrete would contain "…remaining pockets of β-quartz residues that are under strain." and affirm that "This can lead to future fracturing." (*op. cit.,* p. 57). Previously published data and our study clearly refute these two statements. We argue that the association of surface gloss and phase transition cannot be maintained. The α- to β-quartz transition is known to take place at a fairly narrow temperature interval close to 573 °C (Bragg and Gibbs 1925; van Tendeloo et al. 1976; Bachheimer 1980; Dolino et al. 1984). Most silcrete heat treatment experiments describe surface gloss or lustre on the fracture surfaces of freshly flaked silcrete that was heated to temperatures well below 573 °C (Brown et al. 2009; Rowney and White 1997; Schmidt et al. 2013b, 2015; Corkill 1997; Domanski and Webb 1992). Our results also document that micro-roughness on fresh fracture surfaces must be understood in terms of the rocks' mechanical properties, rather than the quartz phase inversion. The loss of roughness on fresh flaking scars is more pronounced in samples with stronger SiOH and K_{Ic} loss, suggesting that the origin of smoother, or glossier, fracture surfaces after heat treatment lies in the water-related crystallographic and mechanical transformations of the rocks. Concerning Wadley and Prinsloo's claim that β-quartz persists in silcrete after cooling down to room temperature, it must be noted that this interpretation contradicts a large number of studies published by physicists and crystallographers, all showing that the phase transition is entirely reversible (Bragg and Gibbs 1925; van Tendeloo et al. 1976; Bachheimer 1980; Dolino et al. 1984). Wadley and Prinsloo suggest that internal strain stabilises β-quartz at low temperatures. A look at the pressure and temperature-dependant phase diagram (P/T-diagram) of the SiO_2 system may shed light on this suggestion. The slope of the α- to β-quartz transition in such a P/T-diagram is positive (Mirwald and Massonne 1980). This means that increasing pressure stabilises α-quartz up until higher temperatures, excluding that compressive residual stresses in a rock would be able to cause stable or metastable β-quartz at low temperatures. Tensional stress could stabilise β-quartz at low temperatures but it can be followed from the relatively steep slope representing the phase transition in the SiO_2 P/T-diagram (Mirwald and Massonne 1980) that ~ 1700 MPa of tensional stress would be necessary. Confirming previous findings

(Domanski et al. 1994; Morrell 1985), all our silcrete samples were found to have fracture strengths below 100 MPa and the chert sample of < 200 MPa (i.e. silcrete breaks at tensional stresses below 100 MPa and chert below 200 MPa). It therefore appears unlikely that metastable β-quartz would be preserved at room temperature (except for "stuffed-derivatives" with a composition other than pure SiO_2) and that such a mechanism may affect the fracture behaviour of silcrete (Wadley and Prinsloo 2014, p. 57). Even at temperatures above 600 °C did we observe no impact of the quartz phase transition on the mechanical properties of our samples: K_{Ic} values recorded in both silcrete samples heated above the transition were identical, within the experimental error, as values recorded below the transition. These results indicate no deterioration of knapping quality or stronger internal fracturing as compared to before the inversion. For all these reasons, we argue that, even if temperatures of > 573 °C had been reached in the MSA, the α- to β-quartz transition is of no importance for our understanding of archaeological stone heat treatment. Heat-induced fracturing during heat treatment must be explained differently. The mechanism of heat-induced fracturing was investigated in another work by Schmidt (2014). This experimental study showed that chert fractures during heat treatment because of critical high-temperature-vapour pressure in fluid inclusions that cannot be released from the structure. The study demonstrated that heterogeneous thermal expansion plays no role in such heat-induced fracturing of chert. So far, there is no similar experimental work about silcrete but, at our current state of knowledge, vapour pressure also appears to be the most probable mechanism of heat-induced fracturing in silcrete.

Conclusion and implications for archaeologic science

Our results allow to propose a comprehensive model of the mechanical transformations taking place upon heat treatment in silica rocks. Stone knapping consists in fracturing rocks in a controlled way to obtain the desired end-products (flakes, blades, etc.). The processes taking place during knapping can be understood by looking at a schematic 2D representation of the atomic structure of a silica rock (chert or silcrete) (Fig. 8). Such silica rocks consist of an agglomerate of partially intergrown quartz crystals (nano-meter sized in the chalcedony of chert and μm- to mm-sized in silcrete). These polycrystalline structures contain defect zones, for example at low-angle grain boundaries or at crystal defect zones, where Si–O–Si bonds cannot be realised across crystals or crystal domains (Micheelsen 1966; Miehe et al. 1984). At these defects, hydroxyl is built into the structure and the resulting surface SiOH groups constitute physical flaws in the rocks (Kronenberg 1994; Graetsch et al. 1987) (Fig. 8a). Upon knapping, a pre-existing micro-fracture or flaw in the rock is developing into a

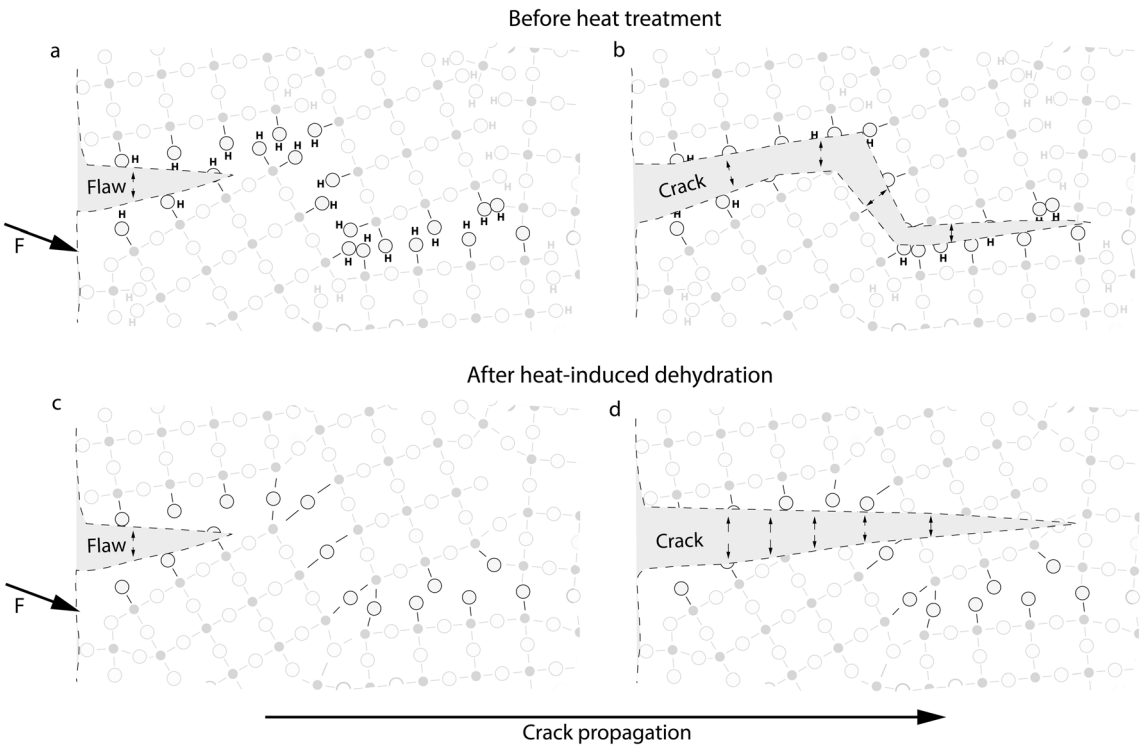

Fig. 8 Two-dimensional schematic representation of the hypothetical crack propagation before and after heat treatment-induced defect healing in silica rocks. A detailed description of this figure can be found in section 5 of the main text

crack that propagates through the structure, eventually leading to the detachment of the desired flake. At least at some places, this propagating crack will follow the direction of OH-related physical flaws in the structure, which are acting as a sort of predetermined breaking points, and is deflected from its ideal propagation direction (Fig. 8b). Continuing this thought experiment, it can be seen that a fracture meandering along such a pathway of flaws is leaving behind a rough surface. Crack deflection and branching are well-known toughening mechanisms that lead to higher fracture toughness or resistance of such a rock (Ritchie 1999). When this rock is heat-treated, SiOH is lost and new Si–O–Si bonds are formed where this is possible geometrically (Schmidt et al. 2011, 2012b) (Fig. 8c). Some of the physical flaws within the rock are lost in this way (i.e. defect healing), reducing the number and size of predetermined breaking points. This reduction of physical flaws is documented by the rising Weibull modulus of heat-treated samples. A fracture propagating in such a heat-treated rock is therefore less offset from its ideal fracture path, i.e. it is less meandering, and the surfaces left behind by the crack are smoother (Fig. 8c). The loss of such toughening mechanisms is documented by our laser scanning microscope measurements that showed the reduction of fracture surface roughness and by our indentation fracture resistance measurements that implied the loss of fracture toughness. This model of the mechanical transformations in chert and silcrete and the correlation of our mechanical data with the published chemical data strengthen the hypothesis (Schmidt et al. 2012b, 2013b) that SiOH loss and subsequent defect healing are the cause of the improvement of knapping quality in chert and silcrete. Regarding these mechanical transformations, the same processes take place in chert and silcrete. Only their magnitude is greater in chert. The reason for this is interpreted to be the presence of silcrete's quartz clasts with mechanical properties invariable upon heat treatment. Because stone tool knapping cracks must run through both cement and these clasts, it is the fracture toughness of these quartz clasts that sets the limit of the achievable transformation's magnitude.

Chert was heat-treated in many parts of the world and during time periods ranging from ~ 20 ka ago to sub-recent times (see for example Tiffagom 1998; Wilke et al. 1991; Eriksen 1997; Flenniken 1987; Léa 2005; Hester 1972). Silcrete was heat-treated since the first occurrence of the technique (~ 160 ka ago) until sub-recent periods in southern Africa and Australia (see for example Brown et al. 2009; Schmidt et al. 2015; Porraz et al. 2016; Hanckel 1985; Flenniken and White 1983; Hiscock 1993; Cochrane et al. 2012). Our results therefore have implications for those archaeological time periods during which heat treatment of either of both rocks was practised, and especially for the comparison of what stone heat treatment implied for the peoples living during these periods.

Acknowledgements We thank S. Schafflick, B. Maier and Brecht GmbH in Wannweil for their assistance with sample preparation, V. Léa for providing chert sample VC-12-05 and J. Plasket for her assistance with collecting the three WK-13- silcrete samples.

Funding information This study was financially supported by the Deutsche Forschungsgemeinschaft (DFG) of the research project *Heat Treatment in the South African MSA* that made the present study possible (Grant Nr: CO 226/25-1, MI 1748/2-1, NI 299/25-1 and SCHM 3275/2-1).

References

Angel RJ, Jackson JM, Reichmann HJ, Speziale S (2009) Elasticity measurements on minerals: a review. Eur J Mineral 21(3):525–550

Asmani M, Kermel C, Leriche A, Ourak M (2001) Influence of porosity on Young's modulus and Poisson's ratio in alumina ceramics. J Eur Ceram Soc 21(8):1081–1086

Bachheimer JP (1980) An anomaly in the β phase near the α-β transition of quartz. J Phys Lett 41(23):559–561

Bleed P, Meier M (1980) An objective test of the effects of heat treatment of Flakeable stone. Am Antiq 45(3):502–507

Bordes F (1969) Traitement thermique du silex au Solutréen. Bull Soc Préhist Fr 66(7):197

Bragg W, Gibbs RE (1925) The structure of α and β quartz. Proc R Soc London Ser A 109(751):405–427

Brown KS, Marean CW, Herries AIR, Jacobs Z, Tribolo C, Braun D, Roberts DL, Meyer MC, Bernatchez J (2009) Fire as an engineering tool of early modern humans. Science 325(5942):859–862

Cady SL, Wenk HR, Sintubin M (1998) Microfibrous quartz varieties: characterization by quantitative X-ray texture analysis and transmission electron microscopy. Contrib Mineral Petrol 130(3):320–335

Cayeux L (1929) Les Roches sédimentaires de France. Roches siliceuses, vol 1. Impr. Nat., Paris

Cochrane GWG, Habgood PJ, Doelman T, Herries AIR, Webb JA (2012) A progress report on research into stone artefacts of the southern Arcadia Valley, Central Queensland. Aust Archaeol 75:104–109

Corkill T (1997) Red, yellow and black: colour and heat in archaeological stone. Aust Archaeol 45:54–55

Crabtree DE, Butler BR (1964) Notes on experiment in Flint knapping: 1 heat treatment of silica materials. Tebiwa 7:1–6

Danzer R, Lube T, Rasche S (2016) On the development of experimental methods for the determination of fracture mechanical parameters of ceramics. In: Hütter G, Zybell L (eds) Recent trends in fracture and damage mechanics. Springer International Publishing, Cham, pp 197–214. https://doi.org/10.1007/978-3-319-21467-2_8

Dejoie C, Tamura N, Kunz M, Goudeau P, Sciau P (2015) Complementary use of monochromatic and white-beam X-ray micro-diffraction for the investigation of ancient materials. J Appl Crystallogr 48(5):1522–1533. https://doi.org/10.1107/S1600576715014983

Delagnes A, Schmidt P, Douze K, Wurz S, Bellot-Gurlet L, Conard NJ, Nickel KG, van Niekerk KL, Henshilwood CS (2016) Early evidence for the extensive heat treatment of Silcrete in the Howiesons Poort at Klipdrift shelter (layer PBD, 65 ka), South Africa. PLoS One 11(10):e0163874. https://doi.org/10.1371/journal.pone.0163874

DIN EN 843 2 (2006) Hochleistungskeramik -Mechanische Eigenschaften monolithischer Keramik bei Raumtemperatur - Teil, vol 2. Bestimmung des Elastizitätsmoduls, Schubmoduls und der Poissonzahl. Beuth Verlag, Berlin

Dolino G, Bachheimer JP, Berge B, Zeyen CME (1984) Incommensurate phase of quartz : I. elastic neutron scattering. J Phys 45(2):361–371

Domanski M, Webb JA (1992) Effect of heat treatment on siliceous rocks used in prehistoric lithic technology. J Archaeol Sci 19(6):601–614
Domanski M, Webb JA, Boland J (1994) Mechanical properties of stone artefact materials and the effect of heat treatment. Archaeometry 36(2):177–208
Domanski M, Webb J, Glaisher R, Gurba J, Libera J, Zakoscielna A (2009) Heat treatment of polish flints. J Archaeol Sci 36(7): 1400–1408
Ebright CA (1987) Quartzite petrography and its implications for prehistoric use and archeological analysis. Archaeol East N Am 15:29–45
Eriksen BV (1997) Implications of thermal pre-treatment of chert in the German Mesolithic. In: Schild R, Sulgostowska Z (eds) Man and Flint, proceedings of the VII international Flint symposium Warszawa-Ostrowiec Swietokrzyski, September 1995. Institute of Archaeology and Ethnology Polish Academy of Sciences, Warsaw, pp 325–329
Flenniken J (1987) The Paleolithic Dyuktai pressure blade technique of Siberia. Arct Anthropol 24:117–132
Flenniken JJ, Garrison EG (1975) Thermally altered Novaculite and stone tool manufacturing techniques. J Field Archaeol 2:125–131
Flenniken JL, White JP (1983) Heat treatment of siliceous rocks and its implication for Australian prehistory. Aust Aborig Stud 1:43–48
Flörke OW, Köhler-Herbertz B, Langer K, Tönges I (1982) Water in microcrystalline quartz of volcanic origin: agates. Contrib Mineral Petrol 80(4):324–333
Flörke OW, Graetsch H, Martin B, Roller K, Wirth R (1991) Nomenclature of micro- and non-crystalline silica minerals, based on structure and microstructure. Neues Jb Mineral Abh 163(1):19–42
Füchtbauer H (1988) Sedimente und Sedimentgesteine, 4th edn. Schweizerbart, Stuttgart
Fukuda J, Yokoyama T, Kirino Y (2009) Characterization of the states and diffusivity of intergranular water in a chalcedonic quartz by high-temperature in situ infrared spectroscopy. Mineral Mag 73(5): 825–835. https://doi.org/10.1180/minmag.2009.073.5.825
Graetsch H, Flörke OW, Miehe G (1985) The nature of water in chalcedony and opal-C from brazilian agate geodes. Phys Chem Miner 12(5):300–306
Graetsch H, Flörke OW, Miehe G (1987) Structural defects in microcrystalline silica. Phys Chem Miner 14(3):249–257
Griffith AA (1921) The phenomena of rupture and flow in solids. Philos Trans R Soc Lond A 221:163–198
Griffiths DR, Bergman CA, Clayton CJ, Ohnuma K, Robins GV (1987) Experimental investigation of the heat treatment of flint. In: Sieveking GG, Newcomer MH (eds) The human uses of flint and chert, Proceedings of the fourth international flint symposium held at Brighton Polytechnic 10-15 April 1983. Cambridge University Press, Cambridge, pp 43–52
Hanckel M (1985) Hot rocks: heat treatment at Burrill Lake and Currarong, New South Wales. Archaeol Ocean 20(3):98–103
Hester TR (1972) Ethnographic evidence for the thermal alteration of siliceous stone. Tebiwa 15:63–65
Hiscock P (1993) Bondian technology in the Hunter Valley, New South Wales. Archaeol Ocean 28:65–76
Hurst S, Cunningham D, Johnson E (2015) Experiments in late archaic methods of heat-treating Ogallala formation quartzarenite clasts along the southern High Plains eastern escarpment of Texas. J Archaeol Sci Rep 3:207–215. https://doi.org/10.1016/j.jasrep.2015.06.006
Inizan ML, Tixier J (2001) L'émergence des arts du feu : le traitement thermique des roches siliceuses. Paléorient 26(2):23–36
Inizan ML, Roche H, Tixier J (1976) Avantages d'un traitement thermique pour la taille des roches siliceuses. Quaternaria Roma 19:1–18
Kerkhof F, Müller-Beck H (1996) Zur bruchmechanischen Deutung der Schlagmarken an Steingeräten. Glastech Ber 42:439–448
Kononenko AV, Kononenko NA, Kajiwara H (1998) Implications of heat treatment experiments on lithic materials from the Zerkalnaya River basin in the Russian Far East. Proc SCA 11:19–25
Kronenberg AK (1994) Hydrogen speciation and chemical weakening of quartz. In: Heaney PJ, Prewitt CT, Gibbs GV (eds) Silica: physical behaviour, geochemistry and materials applications, Reviews in Mineralogy, vol 29. Mineralogical Society of America, Washington, pp 123–176
Léa V (2005) Raw, pre-heated or ready to use: discovering specialist supply systems for flint industries in mid-Neolithic (Chassey culture) communities in southern France. Antiquity 79:1–15
Léa V, Roque-Rosell J, Binder D, Sciau P, Pelegrin J, Regert M, Torchy L, Vaquer J, Cousture M-P, Roucau C (2012) Craft specialization and exchanges during the southern Chassey culture: an integrated archaeological and material sciences approach. In: Colloque international networks in the Neolithic exchange of raw materials, products and ideas in the Western Mediterranean-VII°-III° millennium BC, Février 2011, Barcelona, Spain, pp 119–127
Mandeville MD (1973) A consideration of the thermal pretreatment of chert. Plains Anthropol 18:177–202
Marean CW (2015) An evolutionary anthropological perspective on modern human origins. Annu Rev Anthropol 44:533–556
McBrearty S, Brooks AS (2000) The revolution that wasn't: a new interpretation of the origin of modern human behavior. J Hum Evol 39(5):453–563. https://doi.org/10.1006/jhev.2000.0435
Micheelsen H (1966) The structure of dark flint from Stevns, Denmark. Medd Dansk Geol Foren 16:285–368
Miehe G, Graetsch H, Flörke OW (1984) Crystal structure and growth fabric of length-fast chalcedony. Phys Chem Miner 10(5):197–199
Milot J, Siebenaller L, Béziat D, Léa V, Schmidt P, Binder D (2017) Formation of fluid inclusions during heat treatment of Barremo-Bedoulian Flint: Archaeometric implications. Archaeometry 59(3): 417–434
Mirwald PW, Massonne H-J (1980) The low-high quartz and quartz-Coesite transition to 40 kbar between 600°C and 1600°C and some reconnaissance data on the effect of NaAlO2 component on the low quartz-Coesite transition. J Geophys Res 85(B12):6983–6990
Morrell R (1985) Handbook of properties of technical and engineering ceramics. H.M.S.O, London
Mourre V, Villa P, Henshilwood CS (2010) Early use of pressure flaking on lithic artifacts at Blombos cave, South Africa. Science 330(6004):659–662
Munz D, Fett T (1989) Ceramics: Mechanical Properties, Failure Behaviour, Materials Selection, vol 36. Springer Series in Materials Science, Berlin
Nash DJ, Ullyott JS (2007) Silcrete. In: Nash DJ, McLaren SJ (eds) Geochemical sediments and landscapes. John Wiley, Chichester, pp 95–143
Niihara K, Morena R, Hasselman DPH (1982) Evaluation of KIC of brittle solids by the indentation method with low crack-to-indentation ratios. J Mater Sci Lett 1(1):13–16
Pais JC, Harvey JT (2012) Four point bending. Taylor & Francis, Leiden
Porraz G, Texier P-J, Archer W, Piboule M, Rigaud J-P, Tribolo C (2013) Technological successions in the middle stone age sequence of Diepkloof rock shelter, Western cape, South Africa. J Archaeol Sci 40(9):3376–3400. https://doi.org/10.1016/j.jas.2013.02.012
Porraz G, Igreja M, Schmidt P, Parkington JE (2016) A shape to the microlithic Robberg from Elands Bay cave (South Africa). South Afr Humanit 29:203–247
Purdy BA (1974) Investigations concerning the thermal alteration of silica minerals: an archaeological approach. Tebiwa 17:37–66
Purdy BA, Brooks HK (1971) Thermal alteration of silica minerals: an archeological approach. Science 173(3994):322–325
Rios S, Salje EKH, Redfern SAT (2001) Nanoquartz vs. macroquartz: a study of the a - ß phase transition. Eur Phys J B 20:75–83

Ritchie RO (1999) Mechanisms of fatigue-crack propagation in ductile and brittle solids. Int J Fract 100(1):55–83. https://doi.org/10.1023/A:1018655917051

Roberts DL (2003) Age, genesis and significance of south african coastal belt silcretes, memoir 95. Council for Geoscience, Pretoria

Rowney M, White JP (1997) Detecting heat treatment on Silcrete: experiments with methods. J Archaeol Sci 24(7):649–657

Schindler DL, Hatch JW, Hay CA, Bradt RC (1982) Aboriginal thermal alteration of a Central Pennsylvania Jasper: analytical and behavioral implications. Am Antiq 47(3):526–544

Schmidt P (2014) What causes failure (overheating) during lithic heat treatment? Archaeol Anthropol Sci 6(2):107–112

Schmidt P, Mackay A (2016) Why was Silcrete heat-treated in the middle stone age? An early transformative Technology in the Context of raw material use at Mertenhof rock shelter, South Africa. PLoS One 11(2):e0149243. https://doi.org/10.1371/journal.pone.0149243

Schmidt P, Badou A, Fröhlich F (2011) Detailed FT near-infrared study of the behaviour of water and hydroxyl in sedimentary length-fast chalcedony, SiO2, upon heat treatment. Spectrochim Acta A Mol Biomol Spectrosc 81(1):552–559

Schmidt P, Bellot-Gurlet L, Slodczyk A, Fröhlich F (2012a) A hitherto unrecognised band in the Raman spectra of silica rocks: influence of hydroxylated Si–O bonds (silanole) on the Raman moganite band in chalcedony and flint (SiO_2). Phys Chem Miner 39(6):455–464. https://doi.org/10.1007/s00269-012-0499-7

Schmidt P, Masse S, Laurent G, Slodczyk A, Le Bourhis E, Perrenoud C, Livage J, Fröhlich F (2012b) Crystallographic and structural transformations of sedimentary chalcedony in flint upon heat treatment. J Archaeol Sci 39(1):135–144

Schmidt P, Léa V, Sciau P, Fröhlich F (2013a) Detecting and quantifying heat treatment of flint and other silica rocks: a new non-destructive method applied to heat-treated flint from the Neolithic Chassey culture, southern France. Archaeometry 55(5):794–805

Schmidt P, Porraz G, Slodczyk A, Bellot-Gurlet L, Archer W, Miller CE (2013b) Heat treatment in the south African middle stone age: temperature induced transformations of silcrete and their technological implications. J Archaeol Sci 40(9):3519–3531

Schmidt P, Slodczyk A, Léa V, Davidson A, Puaud S, Sciau P (2013c) A comparative study of the thermal behaviour of length-fast chalcedony, length-slow chalcedony (quartzine) and moganite. Phys Chem Miner 40(4):331–340. https://doi.org/10.1007/s00269-013-0574-8

Schmidt P, Porraz G, Bellot-Gurlet L, February E, Ligouis B, Paris C, Texier JP, Parkington JE, Miller CE, Nickel KG, Conard NJ (2015) A previously undescribed organic residue sheds light on heat treatment in the middle stone age. J Hum Evol 85:22–34

Schmidt P, Paris C, Bellot-Gurlet L (2016) The investment in time needed for heat treatment of flint and chert. Archaeol Anthropol Sci 8(4):839–848

Schmidt P, Lauer C, Buck G, Miller CE, Nickel KG (2017a) Detailed near-infrared study of the 'water'-related transformations in silcrete upon heat treatment. Phys Chem Miner 44(1):21–31. https://doi.org/10.1007/s00269-016-0833-6

Schmidt P, Nash DJ, Coulson S, Göden MB, Awcock GJ (2017b) Heat treatment as a universal technical solution for silcrete use? A comparison between silcrete from the Western cape (South Africa) and the Kalahari (Botswana). PLoS One 12(7):e0181586

Sealy J (2009) Modern behaviour in ancient south Africans: evidence for the heat treatment of stones in the middle stone age. S Afr J Sci 105:323–324

Shippee JM (1963) Was Flint annealed before flaking? Plains Anthropol 8(22):271–272

Sollberger JB, Hester TR (1973) Some additional data on the thermal alteration of siliceous stone. Bull Okla Anthrop Soc 21:181–185

Summerfield MA (1981) The nature and occurrence of Silcrete, southern Cape Province, South Africa. South Africa School of Geography Research Paper 28, University of Oxford

Summerfield MA (1983) Petrography and diagenesis of silcrete from the Kalahari Basin and cape coastal zone, southern Africa. J Sediment Res 53(3):895–909

Thiry M (1991) Pedogenic and groundwater silcretes at Stuart Creek opal field, South Australia. J Sediment Res 61(1):111

Tiffagom M (1998) Témoignages d'un traitement thermique des feuilles de laurier dans le Solutréen supérieur de la grotte du Parpalló (Gandia, Espagne). Paléo 10:147–161

Tixier J, Inizan M-L, Roche H, Dauvois M (1980) Préhistoire de la pierre taillée. I Terminologie et technologie. Cercle de Recherches et d'Etudes Préhistoriques, Antibes

Tognana S, Salgueiro W, Somoza A, Marzocca A (2010) Measurement of the Young's modulus in particulate epoxy composites using the impulse excitation technique. Mater Sci Eng A 527(18–19):4619–4623. https://doi.org/10.1016/j.msea.2010.04.083

Tucker ME (1991) Sedimentary petrology, an introduction to the origin of sedimentary rocks, 2nd edn. Blackwell scientific publications, Oxford

van Tendeloo G, Landuyt J, Amelinckx S (1976) The $\alpha \rightarrow \beta$ phase transition in quartz and AlPO4 as studied by electron microscopy and diffraction. Phys Status Solidi A 33(2):723–735

Wachtman J, Cannon W, Matthewson M (2009) Mechanical properties of ceramics. Wiley, Hoboken

Wadley L (2013) Recognizing complex cognition through innovative Technology in Stone age and Palaeolithic Sites. Camb Archaeol J 23(02):163–183

Wadley L, Prinsloo LC (2014) Experimental heat treatment of silcrete implies analogical reasoning in the middle stone age. J Hum Evol 70(0):49–60

Weibull W (1951) A statistical distribution function of wide applicability. J Appl Mech 18:293–297

Wilke PJ, Flenniken J, Ozbun TL (1991) Clovis Technology at the Anzick Site, Montana. J Calif Gt Basin Anthropol 13(2):242–272

Yonekura K (2010) Experimental study on heat alteration of Palaeolithic material: preliminary results from shale in the northeastern region of Japan. Asian Perspect 49(2):348–362